crystals

MDPI

Article

Nanocrystalline Sulfided NiMoW Catalyst Supported on Mesoporous Aluminas for the Hydrodesulfurization of 4,6-Dimethyldibenzothiophene

Radostina Palcheva [1,*], Luděk Kaluža [2,*], Tanya Petrova [1], Lubomir Dimitrov [3], Daniela Karashanova [4], Georgi Tyuliev [1] and Květuše Jirátová [2]

[1] Institute of Catalysis, Bulgarian Academy of Sciences, Acad. G. Bonchev St., Bldg. 11, 1113 Sofia, Bulgaria; silberbarren@abv.bg (T.P.); tyuliev@ic.bas.bg (G.T.)
[2] Institute of Chemical Process Fundamentals, Czech Academy of Sciences, 165 02 Prague, Czech Republic; jiratova@icpf.cas.cz
[3] Institute of General and Inorganic Chemistry, Bulgarian Academy of Sciences, 1113 Sofia, Bulgaria; dddimitrov_1@abv.bg
[4] Institute of Optical Materials and Technologies, Bulgarian Academy of Sciences, Acad. G. Bonchev St., Bldg. 109, 1113 Sofia, Bulgaria; dkarashanova@yahoo.com
* Correspondence: radost@ic.bas.bg (R.P.); kaluza@icpf.cas.cz (L.K.); Tel.: +359-29793590 (R.P.); +420-220390270 (L.K.)

Abstract: Tri-metallic NiMoW catalysts prepared by impregnating mesoporous aluminas (pore sizes of ~9 nm and surface areas of ~225 m^2/g) obtained by sol-gel (NiMoW/Al) and hydrothermal ($NiMoW/Al_{HYDT}$) processes were investigated in the hydrodesulfurization (HDS) of thiophene and 4,6-dimethyldibenzothiophene (4,6-DMDBT) at H_2 pressures of 1 MPa and 5.0 MPa, respectively. The supports and catalysts were characterized by N_2 physisorption, X-ray diffraction (XRD), scanning electron microscopy (SEM), ultraviolet-visible diffuse reflectance spectroscopy (UV-Vis DRS), temperature-programmed reduction (TPR), X-ray photoelectron spectroscopy (XPS), and high-resolution transmission electron microscopy (HRTEM). The $NiMoW/Al_{HYDT}$ catalyst, which was the most active in both test HDS reactions, was characterized by a pore size of 7.5 nm, whereas the pore size of the catalyst on sol-gel alumina (NiMoW/Al) was only 4.8 nm. Moreover, the $NiMoW/Al_{HYDT}$ catalyst exhibited reduction peaks shifted to a lower temperature during TPR, indicating weaker metal support interactions, a higher degree of Mo (79%) and W (48%) sulfidation, and an optimal layer slab length distribution of $Mo(W)S_2$ nanocrystals preferentially between 2–4 nm with an average layer stacking of 1.7 compared to the NiMoW/Al counterpart.

Keywords: $Mo(W)S_2$ nanocrystals; sol-gel synthesis; hydrothermal synthesis; mesoporous alumina; HDS of 4,6-DMDBT

Citation: Palcheva, R.; Kaluža, L.; Petrova, T.; Dimitrov, L.; Karashanova, D.; Tyuliev, G.; Jirátová, K. Nanocrystalline Sulfided NiMoW Catalyst Supported on Mesoporous Aluminas for the Hydrodesulfurization of 4,6-Dimethyldibenzothiophene. *Crystals* **2023**, *13*, 543. https://doi.org/10.3390/cryst13030543

Academic Editors: Siaw Foon Lee, Chin Wei Lai and Tien-Chien Jen

Received: 27 February 2023
Revised: 16 March 2023
Accepted: 20 March 2023
Published: 22 March 2023

1. Introduction

Catalytic hydrodesulfurization (HDS) is a primary technology that removes sulfur from crude oil to produce ultra-clean fuels. Traditionally, catalytic hydrodesulfurization of gas oil is performed using bimetallic Ni(Co)-Mo catalytic systems supported on γ-alumina [1,2]. The active phase of HDS catalysts consists of MoS_2 nanocrystals dispersed on γ-alumina and promoted with Ni(Co) atoms. However, these catalysts are not so effective for the deep hydrodesulfurization of crude oil fractions containing refractory compounds, such as 4,6-dimethyldibenzothiophene (4,6-DMDBT), because of their low hydrogenation function [3]. For diesel ultra-deep HDS, supported tri-metallic NiMoW sulfide catalysts have been reported to be more active than supported bi-metallic NiMo(W) sulfide catalysts [4,5]. The catalytic HDS activity also depends on the nature of the support [6]. Indeed, the nature of the support influences the metal–support interactions at the early stage of the preparation and thus modifies the final active site structure [7]. Recent

developments in synthesizing pure or modified mesostructured oxides offer a good support choice for deep HDS, especially mesostructured silica-based materials [8,9]. Mesostructured materials exhibit advantages for catalytic applications, such as a high surface area with a pore size in the mesopore range [10], which facilitates overcoming the diffusion limitations in converting relatively bulky molecules.

However, the literature regarding using mesoporous alumina for HDS reaction is scarce. Kaluza et al. [11,12] investigated highly active Mo and bimetallic Ni(Co)Mo catalysts deposited on organized mesoporous aluminas for HDS of thiophene and benzothiophene. Bejenaru et al. [13] studied CoMo catalysts supported on mesoporous alumina prepared using various Al precursors, templates, and solvents. They found a correlation between the pore volume and the conversion of thiophene.

The investigation of the present work focused on the effect of the support surface and metal-support interaction on the HDS activity of the sulfided mesoporous alumina-supported tri-metallic NiMoW catalysts. The aim was to study the hydrodesulfurization (HDS) of thiophene (TH) and 4,6-dimethyldibenzothiophene (4,6-DMDBT), representing light and heavy crude oils. Two preparation methods (sol-gel and hydrothermal) were applied to synthesize mesoporous alumina. The obtained samples were characterized by N_2 adsorption–desorption isotherms, X-ray diffraction (XRD), diffuse reflectance spectroscopy (UV-vis DRS), X-ray photoelectron spectra (XPS), temperature programmed reduction (TPR), and transmission electron microscopy (HRTEM). The HDS activity of the prepared catalysts was correlated with the results of the characterization techniques.

2. Materials and Methods

2.1. Catalyst Preparation

The first sample of mesoporous alumina (Al) was synthesized by a sol-gel synthesis following the method of Yuan et al. [14]. Briefly, Pluronic P123 (P123, Sigma-Aldrich, St. Louis, MO, USA, M = 5800) was dissolved in ethanol, then 37 wt.% HCl, citric acid, and aluminum isopropoxide were added to the solution with stirring for 5 h. The mixture was placed in an oven at 60 °C, and after two days of aging, the solution became a white solid. Calcination was carried out by slowly increasing the temperature from room temperature to 400 °C (1 °C min^{-1} ramp rate) and heating at 400 °C for 4 h in air. Then, from 400 °C, with a temperature ramp of 10 °C min^{-1}, a high-temperature treatment in air at 600 °C was carried out for 1 h. A second sample of mesoporous alumina (Al_{HYDT}) was prepared according to [15] using the molar composition of the reaction mixture: 1.0 Al[i-But]$_3$:0.010 P123:16.48 C_2H_5OH:51.0 H_2O, applying aluminum tri-sec-butoxide (Merck, M = 246.33, d = 0.96). The initial reaction mixture was allowed to stand for 48 h at 95 °C and then for another 24 h at 150 °C. The sample synthesized under hydrothermal conditions was then filtered, washed, and dried at 60 °C for 10 h and calcined in air at 600 °C for 1 h.

The tri-metallic catalysts (NiMoW/Al and NiMoW/Al_{HYDT}) were synthesized via simultaneous impregnation of the mesoporous alumina supports using ammonium heptamolybdate $(NH_4)_6Mo_7O_{24}{\cdot}6H_2O$, ammonium metatungstate $(NH_4)_6H_2W_{12}O_{40}{\cdot}H_2O$, and nickel nitrate $Ni(NO_3)_2{\cdot}6H_2O$) as metal sources. After drying, the samples were calcined at 400 °C. The nominal metal loadings were 3.0, 8.0, and 13.7 wt.% of Ni, Mo, and W, respectively (Mo/W molar ratio = 1). The Ni/(Mo+W) ratio was 0.32. The loadings were confirmed by AAS.

2.2. Characterization of Solids

The textural properties of the supports and catalysts were evaluated using the Quantachrome Instruments NOVA 1200e equipment at −196 °C. Before the experiments, the samples were outgassed under a vacuum for 16 h at 150 °C. The specific surface area, S_{BET}, was calculated using the Brunauer, Emmett, and Teller (BET) equation, and the total pore volume, V_t, and average pore diameter, D_{av}, were determined at $p/p_0 \approx 0.99$. The pore-size distribution was determined using the Barrett, Joyner, and Halenda (BJH) method using the desorption branch of the isotherm. For X-ray measurements, Bruker AXS 2D

Powder X-ray analyzer with filtered CuKα radiation at 30 kV acceleration and 10 mA current of the X-ray tube, scan step 0.05°, and 1 s accumulation time at each step was used. Scanning electron microscopy (SEM) was performed on Philips SEM 515 apparatus, working at an acceleration of 20 kV. DR UV-Vis spectra were taken with a Thermo Evolution 300 spectrometer equipped with a Praying Mantis diffuse reflectance accessory. Temperature programmed reduction (TPR-H_2) experiments were carried out in the measuring cell of a differential scanning calorimeter (DSC), directly connected to a gas chromatograph (GC), in the 10–700 °C range at a 10 °C min^{-1} heating rate in a flow of H_2/Ar = 1:9, the total flow rate being 20 mL min^{-1}. A cooling trap between DSC and GC removed water produced during the reduction. XPS spectra of oxide, sulfided, and used catalysts were carried out in the analysis chamber of the electron spectrometer ESCALAB–MkII (VG Scientific) with a base pressure of 10^{-8} Pa. The spectra were excited with non-monochromatic AlKα radiation (hν = 1486.6 eV) at a total instrumental resolution of 1.0 eV as measured by the FWHM of the $Ag3d_{5/2}$ photoelectron peak. The O1s peak at 532.7 eV was used as the energy scale reference due to the very low intensity of the C1s line coming from the adventitious carbon on the surface. The local structure and morphology of sulfided tri-metallic samples were observed by JEOL JEM 2100 transmission electron microscope and a JEOL 2100 XEDS: Oxford Instruments, X-MAXN 80 T CCD Camera ORIUS 1000, 11 Mp, GATAN at accelerating voltage of 200 kV.

2.3. Catalyst Activity

The hydrodesulfurization of thiophene (TH) was done in the gas phase using an integral fixed-bed tubular flow microreactor (i.d. 2 mm) at 310, 340, 370 °C, and 1.0 MPa. Prior to the measurements, the catalysts were sulfided in-situ with an H_2S/H_2 flow (1/10) at 400 °C and atmospheric pressure with a temperature ramp of 6 °C min^{-1} and a dwell time of 1 h. The catalyst particle size fraction 0.16–0.32 mm was diluted with an inert α-Al_2O_3 of particle size fraction 0.32–0.50 mm to form a bed length of 20 mm. The catalyst charge, W, was 0.06 g. The most active $NiMoW/Al_{HYDT}$ was also measured at the catalyst charge of 0.01 g. The reaction was run at the feed rate of TH, F_{TH}, 0.909 mmol h^{-1} and feed rate of H_2, F_{H2}, 0.732 mmol h^{-1}. The composition of the feed was kept constant. A steady state was reached in 30 min. No changes in the conversions were observed during the following 90 min. The reaction mixture was analyzed on a Hewlett–Packard gas chromatograph (HP 4890). Butane and thiophene were identified in the reaction products, while the content of tetrahydrothiophene, other organic sulfides, and butenes was negligible. The conversion of thiophene, x_{TH}, was defined as $x_{TH} = (n^0_{TH} - n_{TH})/n^0_{TH}$, where n^0_{TH} and n_{TH} were the initial and final number of TH moles, respectively. The rate constant of TH conversion, k_{TH} ($mmol_{TH}$ g^{-1} h^{-1}), was calculated using an empirical pseudo-first-order rate equation:

$$k_{TH} = -(F_{TH}/W) \ln(1 - x_{TH}). \quad (1)$$

HDS of 4,6-dimethyldibenzothiophene (4,6-DMDBT) was carried out in a fixed-bed flow reactor at 360 °C and 5.0 MPa. The catalysts were pre-sulfided in situ, as described above. The feed consisted of 4,6-DMDBT, decane, and H_2. The composition of the feed was kept constant at 1, 200, and 4799 kPa of 4,6-DMDBT, decane, and H_2, respectively. The reaction was performed at three feed rates, F, of 4,6-DMDBT: 4.6, 6.1, and 9.2 mmol h^{-1}. The catalyst weight, W, was 0.1 and 0.3 g. Additionally, the $NiMoW/Al_{HYDT}$ sample was also measured at W = 0.04 g. The catalyst was diluted with inert α-Al_2O_3 to create the catalyst bed length of 3 cm. The reaction mixture was analyzed on Hewlett-Packard gas chromatographs (HP 6890 Series) equipped with a mass spectrometer (MS) and flame ionization detector (FID).

The products of 4,6-DMDBT transformation are summarized in Figure 1. The conversion of 4,6-DMDBT, $x_{4,6\text{-DMDBT}}$, and the relative content of 4,6-DMDBT, $a_{4,6\text{-DMDBT}}$, were defined as $x_{4,6\text{-DMDBT}} = 1 - a_{4,6\text{-DMDBT}} = (n^0_{4,6\text{-DMDBT}} - n_{4,6\text{-DMDBT}})/n^0_{4,6\text{-DMDBT}}$, where $n^0_{4,6\text{-DMDBT}}$ and $n_{4,6\text{-DMDBT}}$ are the initial and final number of moles of 4,6-DMDBT, respectively. The yield of a reaction product, y_i, was defined as $y_i = n_i/n^0_{4,6\text{-DMDBT}}$, where

$n^0_{4,6\text{-DMDBT}}$ and n_i are the initial number of moles of 4,6-DMDBT and the moles of a reaction product, respectively.

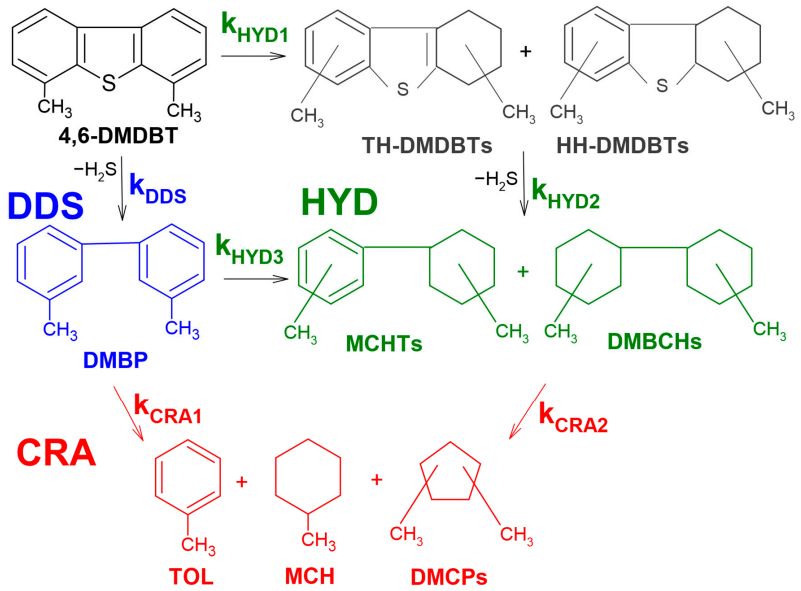

Figure 1. Scheme of 4,6-dimethyldibenzothiophene hydrodesulfurization.

Yields of 4,6-dimethylbiphenyl (y_{DMBP}) were formed by direct-desulfurization (DDS) of 4,6-DMDBT. In contrast, hydrogenation (HYD) of 4,6-DMDBT led to hydrogenated dibenzothiophenes, such as tetrahydro-dibenzothiophenes (TH-DMDBTs) and hexahydro-dibenzothiophenes (HH-DMDBTs) (Figure 1). The yields of hydrogenated dibenzothiophenes were quantified as the sum of the yields of TH-DMDBTs and HH-DMDBTs, $y_{TH\text{-}DMDBTs+HH\text{-}DMDBTs}$. TH-DMDBTs and HH-DMDBTs hydrodesulfurization led to methyl-cyclohexyl-toluenes (MCHTs) and dimethyl-bicyclohexyls (DMBCHs). Methyl-cyclohexyl-toluenes (MCHTs) and dimethyl-bicyclohexyls (DMBCHs) were also formed by 4,6-dimethylbiphenyl (DMBP) hydrogenation. These desulfurized products consisting of 14 carbon atoms and cyclohexane ring were quantified as the sum of the yields MCHTs and DMBCHs ($y_{MCHTs+DMBCHs}$). Furthermore, cracking (CRA) of DMBP, MCHTs, and DMBCHs yielded toluene (TOL), methylcyclohexane (MCH), and dimethyl-cyclopentanes (DMCPs). The yield of the cracked product (y_{C7}) was defined as the sum of the yields of toluene, methylcyclohexane, and dimethylcyclopentanes: $y_{C7} = y_{TOL} + y_{MCH} + y_{DMCPs}$.

Hydrodesulfurized hydrocarbons yield (y_{HDS}) was defined as the sum of C_{14} and C_7 sulfur-free hydrocarbons: $y_{HDS} = y_{DMBP} + y_{MCHTs} + y_{DMBCHs} + y_{TOL} + y_{MCH} + y_{DMCPs}$.

Hydrodesulfurization (HDS) activity was quantified as the empiric pseudo-first-order rate constant k_{HDS} of the sum of the yields of desulfurized hydrocarbons y_{HDS}. The activity k_{HDS} (mmol g^{-1} h^{-1}) was achieved by non-linear fitting from the dependence y_{HDS} on $W/F_{4,6\text{-DMDBT}}$:

$$y_{HDS} = 1 - \exp\left(-k_{HDS} \times W/F_{4,6\text{-DMDBT}}\right). \quad (2)$$

3. Results

3.1. Characterization of the Alumina Supports and Oxidic Catalysts

Figure 2 shows the XRD patterns of the supports and corresponding calcined alumina-supported NiMoW catalysts. A nearly flat XRD pattern of the mesoporous alumina (Al) synthesized by the sol-gel method (calcined at 600 °C) indicates that the sample was amorphous. In contrast, the alumina prepared by the hydrothermal method and calcined at 600 °C (Al_{HYDT}) shows broad peaks around 35–40°, 45°, and 67° 2θ which correspond to the crystalline line of cubic γ-alumina.

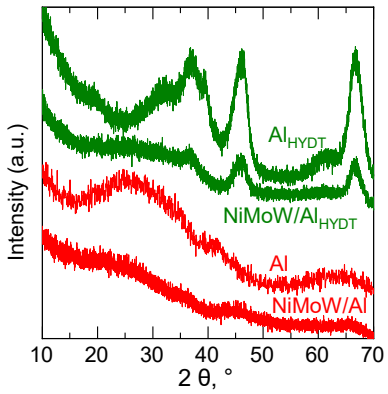

Figure 2. XRD patterns of the investigated Al oxides and calcined alumina-supported NiMoW catalysts.

The XRD pattern of the NiMoW/Al tri-metallic mesoporous alumina-based catalyst does not show crystalline NiMo(W) oxides, indicating that the NiMo(W) oxides are amorphous. These diffractograms are consistent with the diffractograms of the parent supports. The XRD pattern of NiMoW/Al$_{HYDT}$ catalyst slightly copies the pattern of Al$_{HYDT}$, though with lower peak intensities.

The textural properties of the calcined supports and corresponding catalysts are presented in Table 1 and Figure 3. The nitrogen adsorption–desorption isotherms of the studied aluminas are typical of type IV with an H2-type hysteresis loop [16], indicating a mesoporous structure (Figure 3). Both supports show similar values of S_{BET}, V_t, and D_{av} (Table 1), but they differ in the shape of the adsorption–desorption curves, especially in the p/p_0 range of 0.4–0.9, and thus in the pore-size distribution. A relatively steep desorption branch is observed for the alumina Al$_{HYDT}$ (γ-Al_2O_3), demonstrating the occurrence of large mesopores centered on a pore-size distribution curve of approximately 6 nm. In contrast, alumina prepared by the sol-gel method (Al) shows a maximum on its pore-size distribution curve only at approximately 4 nm.

Table 1. Textural parameters S_{BET}, V_t, and D_{av} and HDS activities k_{TH} (340 °C and 1 MPa) and k_{HDS} (360 °C and 5 MPa).

Sample	S_{BET} [m^2 g^{-1}]	V_t [cm^3 g^{-1}]	D_{av} [nm]	k_{TH} [mmol g^{-1} h^{-1}]	k_{HDS} [mmol g^{-1} h^{-1}]
Al	232	0.52	9.0		
Al$_{HYDT}$	217	0.47	8.7		
NiMoW/Al	215 (93) [1]	0.26 (0.15) [1]	4.8 (6.3) [1]	12	1.9
NiMoW/Al$_{HYDT}$	167 (118) [1]	0.31 (0.25) [1]	7.5 (8.6) [1]	94	10.3

[1] the values in parentheses are the used sulfide catalysts after the HDS of 4,6-DMDBT.

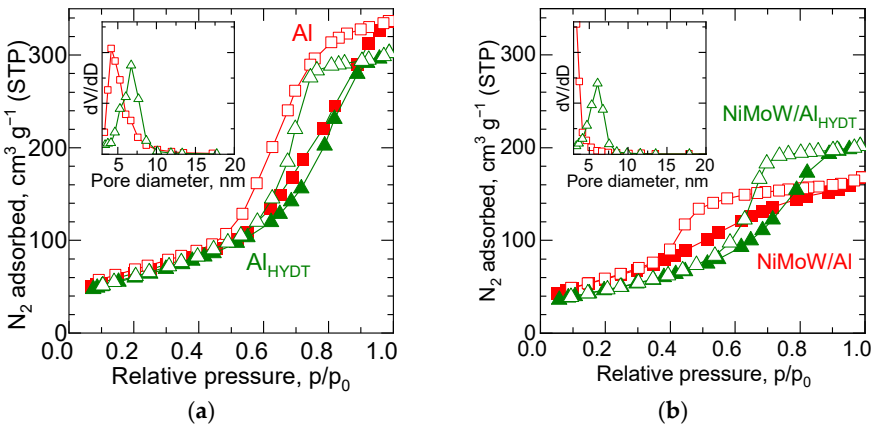

Figure 3. Adsorption–desorption isotherms of N_2 and pore-size distributions: (**a**) Supports; (**b**) Oxidic catalysts.

Typical SEM images in Figure 4a,b depict the surface morphology of porous sol-gel alumina. The particle numbered 1 in Figure 4a has a relatively smooth surface, while number 2 has a rougher surface due to holes in the pores.

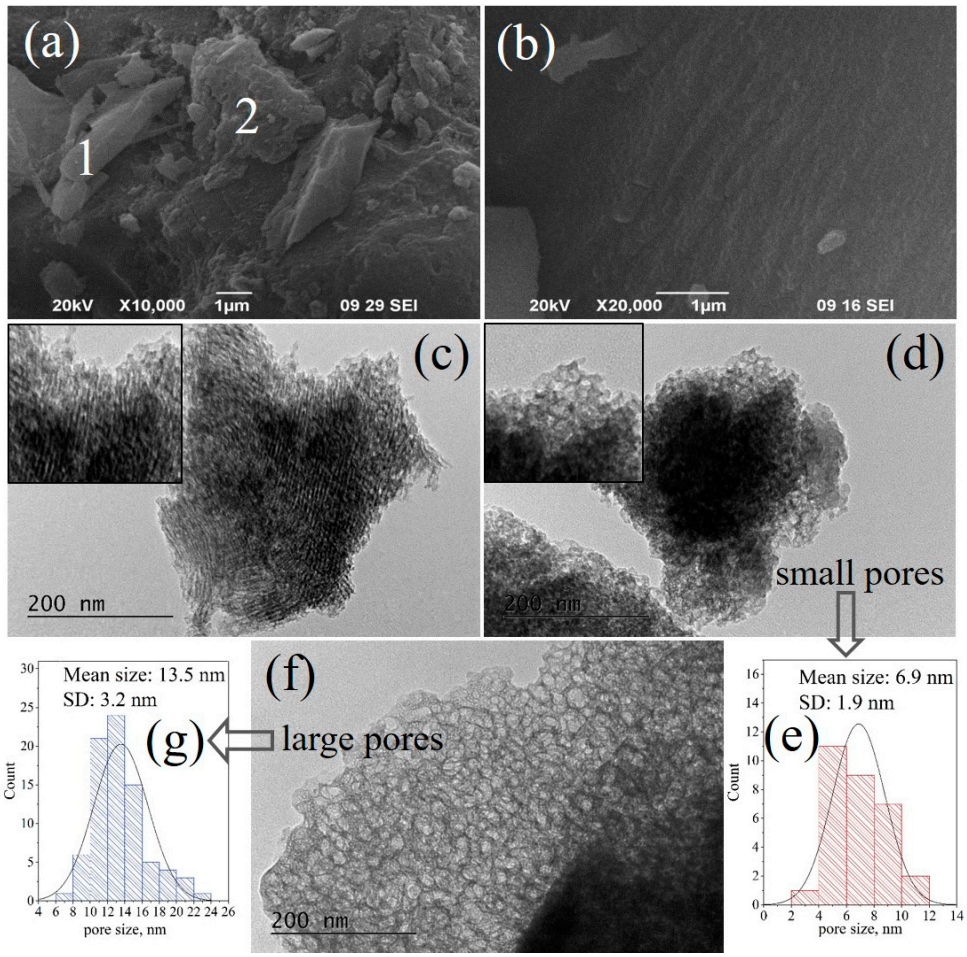

Figure 4. SEM (**a**,**b**) and TEM (**c**,**d**,**f**) micrographs of alumina synthesized using the sol-gel method at 600 °C. The histograms (**e**,**g**) represent the pore-size distribution for small (**d**,**e**) and large (**f**,**g**) pores of the mesoporous Al_2O_3.

Using TEM, the porous structure of Al_2O_3 can be seen even better in Figure 4c,d. The particle in Figure 4c is oriented parallel to the electron beam so that pore channels can be observed. In contrast, the pore holes are directly visible in Figure 4d. Cropped and magnified parts of the Al_2O_3 particles are presented in the insets of the corresponding micrographs for better illustration. The pore-size distributions of the alumina are shown in Figure 4 as histograms. The pore diameters lie in the interval of 2–12 nm with an average size of 6.9 nm. However, pores with larger sizes were also found in Figure 4f. Their diameters range from 6–24 nm, and they have an average size of 13.5 nm, as seen in the histogram in Figure 4g.

Tri-metallic NiMoW catalysts revealed decreased surface area and pore volume after the impregnation/calcination step (Table 1). These decreases in S_{BET} and mainly in pore volume V_t can be due to the filling of the support pores with impregnated metal species [17]. The decrease in the total pore volume was approximately 50% for the NiMoW/Al catalyst (Al_2O_3 prepared by the sol-gel method), whereas the decrease was only approximately 34% for the catalyst prepared on Al_{HYDT} (γ-Al_2O_3 prepared by the hydrothermal method). At the same time, the calculated average pore size D_{av} of 7.5 nm for NiMoW/Al_{HYDT} remained higher than the D_{av} of 4.8 nm for NiMoW/Al (Table 1). The smallest pores (about 3–4 nm) observed on the alumina (Al) support in Figure 3a remained preserved during the

impregnation/calcination step of the catalyst preparation, while their larger pores were filled with active components. In contrast, NiMoW/Al_{HYDT} had the most pore volume centered in the mesopores. These differences are illustrated in Figure 3b.

UV-Vis DR spectra of the prepared tri-metallic catalysts are shown in Figure 5a. The reflections are presented as Kubelka-Munk functions. According to [18,19], absorption bands corresponding to ligand-to-metal charge transfer (LMCT) $O^{2-} \rightarrow Mo(W)^{6+}$ can be observed in the 200–360 nm region. The isolated molybdate (tungstate) species in tetrahedral coordination (Mo(W)(Td)) shows a characteristic absorption band at ~250–280 nm. In contrast, the signal of $Mo(W)^{6+}$ ions in octahedral coordination (Mo(W)(Oh)) as well as of polymeric Mo(W) species is observed between 260 and 330 nm.

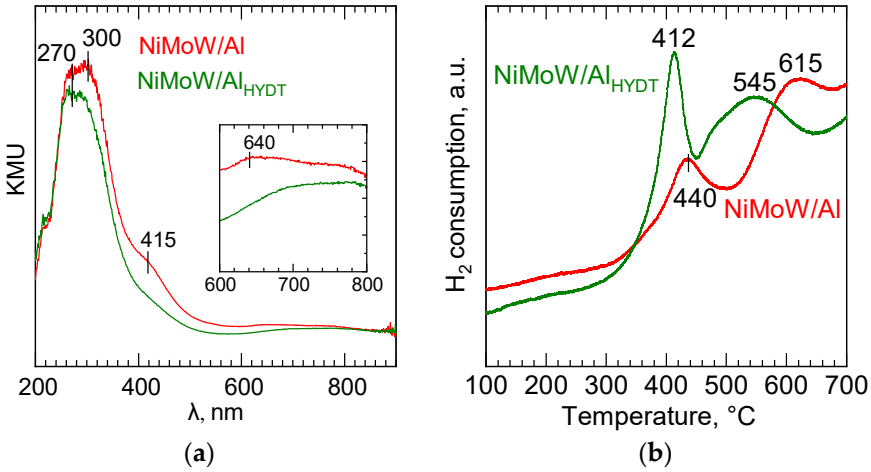

Figure 5. UV-Vis DRS (**a**) and TPR (**b**) of oxidic catalysts.

The above bands can be observed in the spectra of tri-metallic NiMoW catalysts, where mixed octahedral and tetrahedral $Mo(W)^{6+}$-oxo forms occur. The broad bands at 640 and 770 nm in the catalysts could be attributed to the presence of tetrahedral and octahedral coordinated forms of Ni species [20] in the inset in Figure 5a. The NiMoW/Al_{HYDT} sample did not reveal a band at 640 nm, which is attributed to the presence of $NiAl_2O_4$, which is known to be more difficult to sulfide than the octahedral species. Apparently, these species are present in the catalyst containing sol-gel alumina.

The TPR profiles in Figure 5b show the H_2 consumption during the reduction of tri-metallic NiMoW catalysts in the temperature range of 100–700 °C. The catalysts show two main peaks in the temperature range of 415–435 °C and 530–610 °C. The NiMoW/Al_{HYDT} sample shows reduction peaks with a shift of 20–80 °C to lower temperatures compared to the NiMoW/Al sample, indicating weaker metal-support interaction [21,22] in NiMoW/Al_{HYDT}. The presence of W in the trimetallic catalysts apparently contributes to the formation of broad reduction peaks at 545 and 615 °C, which probably form mixed Mo-W oxide phases, thus facilitating the reduction of Mo [23].

3.2. Characterization of Sulfided and Used Catalysts

The oxidation state of the elements in the sulfided and spent alumina-supported NiMoW catalysts was investigated by XPS. The oxidation state of the elements is compared with that of the oxidized form in Table 2. The spectra of the calcined catalysts showed Mo 3d, W 4f, and Ni 2p features characteristic of Mo^{6+}, $W^{6+,}$ and Ni^{2+} in an oxide matrix. The binding energy (BE) of Mo^{6+} that corresponds to Mo $3d_{5/2}$ is 233.3 eV, and the BE of Ni^{2+} that corresponds to the Ni $2p_{3/2}$ line is 856.8 eV. For the NiMoW/Al sample, the BE of the Ni$2p_{3/2}$ line is approximately 0.5 eV higher, indicating a stronger interaction of nickel with the sol-gel alumina support in this sample. The BE of the other chemical components of the catalysts are as follows: W $4f_{7/2}$ = 36.3 eV, Al 2p = 74.8 eV, O 1s = 531.8 eV.

Table 2. Binding energy (eV) of elements in calcined, sulfided, and used catalysts.

Elements	NiMoW/Al	NiMoW/Al_{HYDT}
Calcined catalysts		
$Ni2p_{3/2}$	857.2	856.7
$Mo3d_{5/2}$	233.3	233.0
$W4f_{7/2}$	36.4	36.3
Sulfided catalysts		
$Ni2p_{3/2}$	864.8 NiO_x	863.9 NiO_x
	854.1 NiMo(W)S	853.9 NiMo(W)S
	852.9 NiS_x	852.9 NiS_x
$Mo3d_{5/2}$	234.5 MoO_3	233.7 MoO_3
	232.5 MoO_xS_y	231.7 MoO_xS_y
	229.2 MoS_2	229.0 MoS_2
$W4f_{7/2}$	36.2 WO_3	36.0 WO_3
	32.8 WS_2	32.7 WS_2
$S2p_{3/2}$	162.1 S^{2-}	162.1 S^{2-}
	167.9 SO_4^{2-}	168.2 SO_4^{2-}
Used catalysts		
$Ni2p_{3/2}$	864.7 NiO_x	863.8 NiO_x
	854.0 NiMo(W)S	853.9 NiMo(W)S
	852.9 NiS_x	852.9 NiS_x
$Mo3d_{5/2}$	234.1 MoO_3	233.9 MoO_3
	232.4 MoO_xS_y	232.0 MoO_xS_y
	229.2 MoS_2	229.2 MoS_2
$W4f_{7/2}$	36.3 WO_3	36.2 WO_3
	32.8 WS_2	32.6 WS_2
$S2p_{3/2}$	162.2 S^{2-}	162.1 S^{2-}
	168.5 SO_4^{2-}	168.1 SO_4^{2-}

The Mo 3d spectra of sulfided NiMoW catalysts were deconvoluted into three doublets (Figure 6). Mo $3d_{5/2}$ components were located at BE of 229.2 eV (Mo^{4+} as in MoS_2), 231.7 eV (Mo^{5+} assigned to oxysulfidic MoO_xS_y species) and 233.7 eV (Mo^{6+} as in MoO_3). Contrary to the Mo species, the W 4f signals were fitted, assuming the coexistence of W^{6+} and W^{4+} species. Thus, the W 4f peak at 32.6 eV corresponds to W^{4+} species in a WS_2-like structure, while the BE at 36.2 eV belongs to W^{6+} (WO_3) species [24]. Deconvolution of the Ni $2p_{3/2}$ spectra revealed three major peaks with associated satellites: at 852.9 eV attributed to NiS_x, at 854.0 eV corresponding to the NiMo(W)S phase, and at 863.8–864.7 eV indicating Ni^{2+} ions in oxide matrix. The content of NiMo(W)S phases in NiMoW/Al and NiMoW/Al_{HYDT} reaches 46% and 78%, respectively. The S 2p spectra were fitted with two S 2p doublets: the first peak with BE S $2p_{3/2}$ 161.4 eV corresponds to S^{2-} ions in the MoS_2(WS_2) and/or NiS_x phase, the second at BE = 168.6 eV characterizes the presence of SO_4^{2-} ions on the surface.

The surface exposure of supported Ni, Mo, and W species was estimated from the atomic intensity ratios of NiMoW/Al and NiMoW/Al_{HYDT} catalysts in Table 3. The tungsten species were only partially sulfided in all catalysts since MoO_3 is sulfided faster than WO_3. The degree of Mo sulfidation in the NiMoW/Al catalyst was 66% compared to 79% of the degree of Mo sulfidation in the NiMoW/Al_{HYDT} catalyst. Thus, the NiMoW/Al_{HYDT} catalyst had a greater surface exposure to metal species than the NiMoW/Al catalyst.

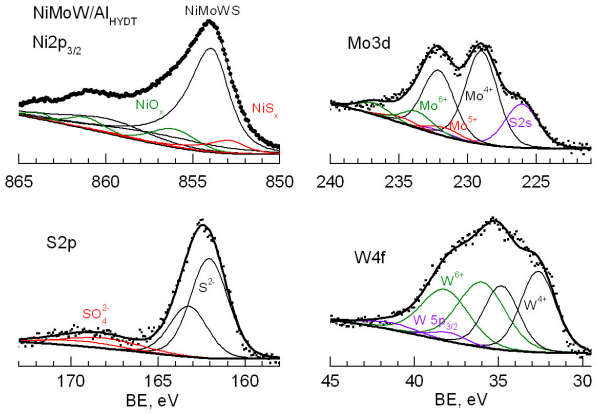

(**a**)

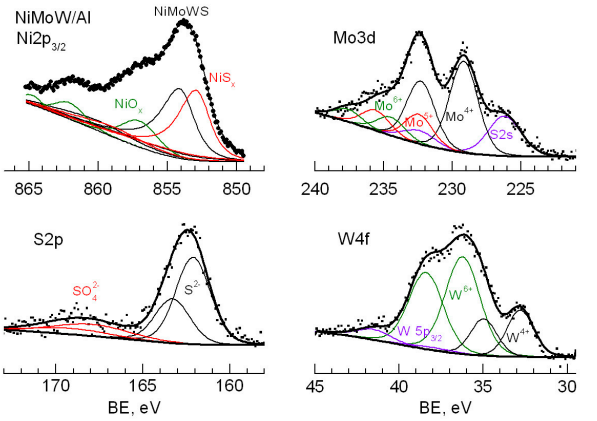

(**b**)

Figure 6. Decomposition of XPS spectra of elements of sulfided NiMoW/Al$_{HYDT}$ (**a**) and NiMoW/Al (**b**) catalysts.

Table 3. Surface atomic ratios of prepared samples.

Samples	Ni/Al	Mo/Al	W/Al	S/Mo	S/W	S/(Ni+Mo+W)	$Mo^{4+}/Mo_{tot.}$, %	$W^{4+}/W_{tot.}$, %
NiMoW/Al								
calcined	0.02	0.05	0.04					
sulfided	0.02	0.04	0.03	2.57	3.22	1.16	66	27
used	0.01	0.03	0.03	2.14	2.65	0.99	61	20
NiMoW/Al$_{HYDT}$								
calcined	0.03	0.06	0.06					
sulfided	0.03	0.06	0.05	3.00	3.93	1.33	79	48
used	0.03	0.06	0.05	2.97	3.64	1.29	74	46

The supported sulfided NiMoW catalysts, fresh and used, were characterized by XRD in Figure 7. The superposition of the broadened diffraction peaks corresponding to the MoS_2 and γ-Al_2O_3 phases complicated the analysis. However, the sulfided NiMoW/Al$_{HYDT}$ catalyst showed striking diffraction reflections at 14.4° (002) and 58° (110) of the MoS_2/WS_2 crystallites [25]. A typical peak observed in the XRD patterns due to the stacking of the MoS_2/WS_2 slabs along c-axes is at $2\theta = 14.4°$ [4]. Also, XRD analysis of the used catalysts did not show any peak that could be attributed to the formation of larger crystals.

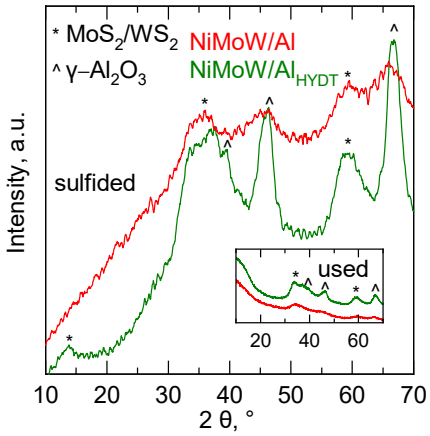

Figure 7. XRD patterns of the catalysts after sulfidation (H_2/H_2S) and the catalytic test (inset).

HRTEM experiments confirmed the formation of mixed sulfides in the sulfided Ni-MoW catalysts. They were detected at selected sites by electron diffraction, as seen in Figure 8. The presence of $Mo_{18}Ni_{4.14}S_{24}$ in a trigonal crystal system was found for the NiMoW/Al sample. The distance between the slabs of this sulfide form was 0.297 nm. The layered structure of the particles was furthermore observed even at low magnifications (40,000×) (Figure 8a). Relatively long curved stacks (more than 20 nm) were observed in Figure 8b. Similar long stacks were previously reported in [3]. In Figure 8d, slabs of approximately 10 nm in length with a typical interlayer distance [26] of 0.59 nm were observed in some regions. Diffraction analysis (Figure 8c) and high-resolution TEM (Figure 8b,d) allow the determination of a set of interplanar distances that show good agreement with the $Mo_{18}Ni_{4.14}S_{24}$ phase when compared to the Crystallography Open Database (COD).

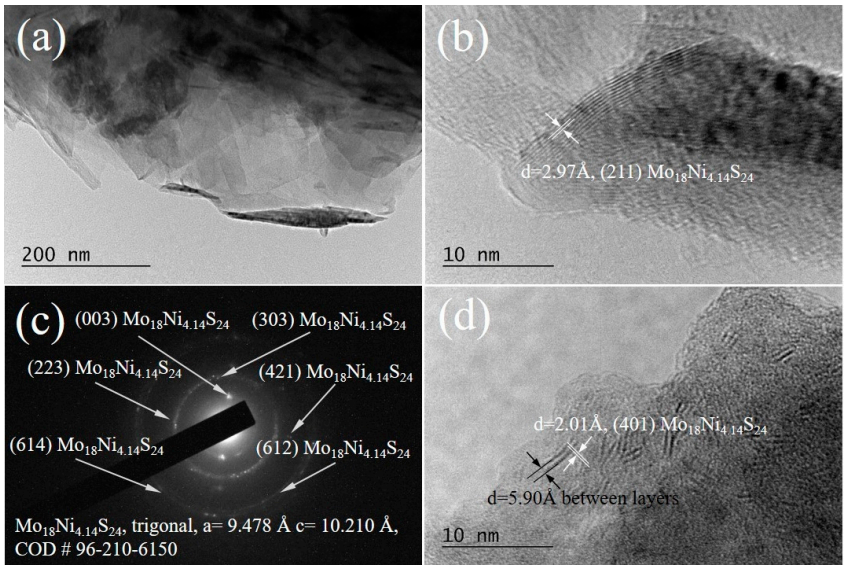

Figure 8. Bright Field TEM micrograph (**a**), HRTEM (**b**), and (**d**) and selected area electron diffraction (**c**) of the NiMoW/Al catalyst sulfided at 400 °C.

The HRTEM investigation also provides an opportunity to estimate the degree of the stacking and dimensions of the active Ni-Mo(W)-S species of the catalysts. Bright Field TEM (a) and HRTEM (b) images of the NiMoW/Al_{HYDT} sulfided at 400 °C are presented in Figure 9, together with the elemental mapping of one particle received by Energy Dispersive Spectroscopy (EDS). As expected, the catalyst displays the typical fringes of MoS_2(WS_2) nanocrystallites after sulfidation. For the NiMoW/Al_{HYDT}, TEM mapping was performed by scanning map. EDS depicts in Figure 9c that the distribution of Mo, W, Ni, and S on the support is uniform.

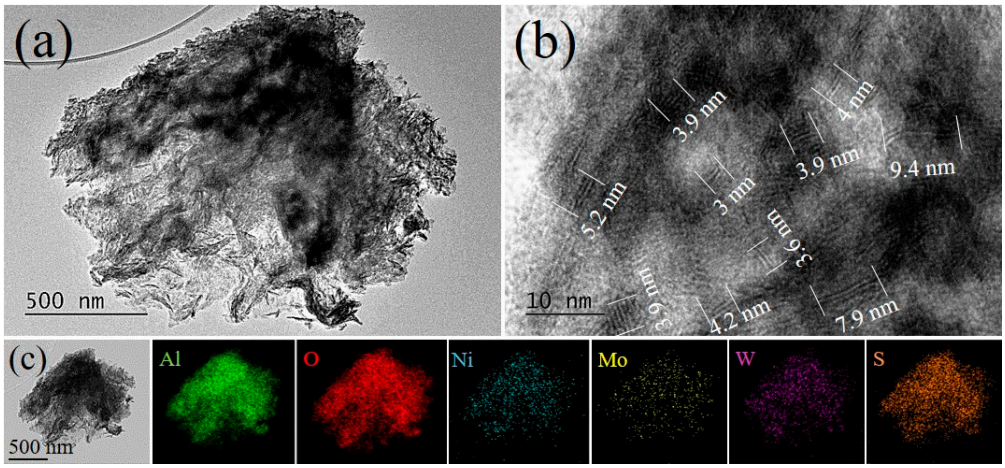

Figure 9. Bright Field TEM (**a**) and HRTEM (**b**) images of the NiMoW/Al_{HYDT} sulfided at 400 °C: (**c**) Scanning mode with the EDS elemental mapping of the same particle as it is presented in (**a**).

The results of the statistical analysis of the active species on these images are presented in Figure 10. Two hundred particles composed of Mo(W)S_2 layers were counted by size and arrangement to allow for statistical analysis. The stacking degree was approximately 1.7, close to the value observed by Hensen et al. [27] for a NiW hydrotreating catalyst. The slab length distribution showed almost the same proportion for slabs with dimensions less than 2 nm and between 2.1 and 4 nm. As previously observed [28], the most active NiMoW/Al_{HYDT} catalyst is characterized by a relatively narrow distribution and a preferential slab length in the 2–4 nm range. In the case of the supported NiMoW/Al_{HYDT} sample, the Ni promoter is probably located at the edge sites of the Mo(W)S_2 layers, forming "NiMo(W)S" phases according to other authors [3,9,17,20].

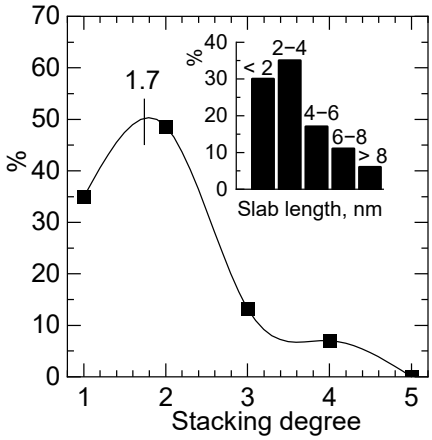

Figure 10. Slab length distribution and layer stacking in the NiMoW/Al_{HYDT}.

The isotherms and the pore-size distributions of the used catalysts are shown in Figure 11. The catalysts analyzed after the catalytic test showed slightly broader pore-size distributions and smaller pore volumes than the oxide samples (Table 1, data in parentheses). The S_{BET} of the used catalysts decreased compared to the S_{BET} of the oxide samples. This decrease was more pronounced for the NiMoW/Al catalyst prepared on sol-gel alumina.

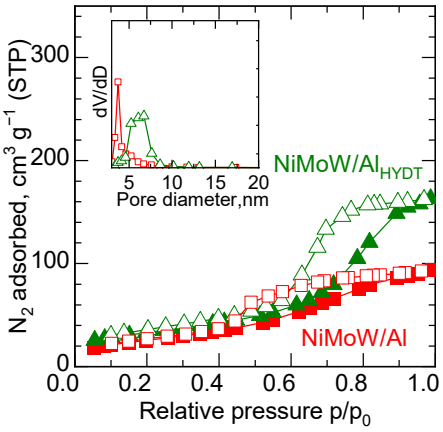

Figure 11. Adsorption–desorption isotherms of N_2 and pore distribution of the used catalysts.

3.3. Catalytic Activity

All catalysts were evaluated for the hydrodesulfurization of thiophene at 310, 340, and 370 °C, and 1 MPa and hydrodesulfurization of 4,6-dimethyldibenzothiophene (4,6-DMDBT) at 360 °C and 5 MPa. The selected activity indices k_{TH} and k_{HDS} are overviewed in Table 1. The activity of the NiMoW/Al_{HYDT} catalyst prepared on the hydrothermally treated alumina in thiophene HDS (k_{TH}) was about 7.8-fold higher at each studied temperature compared to the activity k_{TH} of NiMoW/Al. HDS of refractory 4,6-DMDBT at 5 MPa confirmed the overwhelming activity of NiMoW/Al_{HYDT}. The activity k_{HDS} of NiMoW/Al_{HYDT} was about 5.4 times higher than the k_{HDS} of NiMoW/Al (Figure 12). These results corresponded with the TPR patterns in Figure 5b, where NiMoW/Al_{HYDT} qualitatively differed from the NiMoW/Al catalyst. The method of preparation had thus leading influence on the resultant HDS activity.

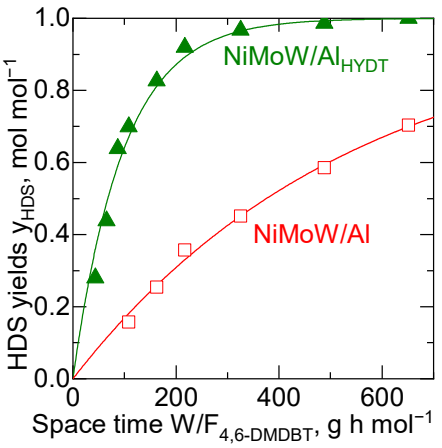

Figure 12. The formation of desulfurized products, y_{HDS}, during HDS of 4,6-dimethyldibenzothiophene at 360 °C and 5 MPa: lines—fitting of the activity k_{HDS} (Table 1) as in Equation (2).

3.4. Selectivity of Catalyst during 4,6-Dimethyldibenzothiophene HDS

To elucidate the catalyst selectivity, a Simplified Reaction Progress Kinetic Analysis (RPKA) was performed in Figure 13. For this purpose, the HDS products of 4,6-DMDBT shown in Figure 1 were classified into four groups. The transformation of 4,6-DMDBT into these groups was described by a parallel-consecutive scheme of six pseudo-first-order rate reactions using the system in Equation (3). Six empirical pseudo-first-order rate constants k_i were fitted to obtain the kinetic curves in Figure 13:

$$
\begin{aligned}
da_{4,6\text{-DMDBT}}/d(W/F_{4,6\text{-DMDBT}}) &= -k_{DDS} \times a_{4,6\text{-DMDBT}} - k_{HYD1} \times a_{4,6\text{-DMDBT}} \\
dy_{DMBP}/d(W/F_{4,6\text{-DMDBT}}) &= k_{DDS} \times a_{4,6\text{-DMDBT}} - k_{CRA1} \times y_{DMBP} \\
dy_{TH\text{-}DMDBTs+HH\text{-}DMDBTs}/d(W/F_{4,6\text{-DMDBT}}) &= k_{HYD1} \times a_{4,6\text{-DMDBT}} - k_{HYD2} \times y_{TH\text{-}DMDBTs+HH\text{-}DMDBTs} \\
dy_{MCHTs+DMBCHs}/d(W/F_{4,6\text{-DMDBT}}) &= k_{HYD2} \times y_{TH(HH)\text{-}DMDBTs} + k_{HYD3} \times y_{DMBP} - k_{CRA2} \times y_{MCHTs+DMBCHs} \\
dy_{TOL+MCH+DMCPs}/d(W/F_{4,6\text{-DMDBT}}) &= k_{CRA1} \times y_{DMBP} + k_{CRA2} \times y_{MCHTs+DMBCHs}
\end{aligned}
\tag{3}
$$

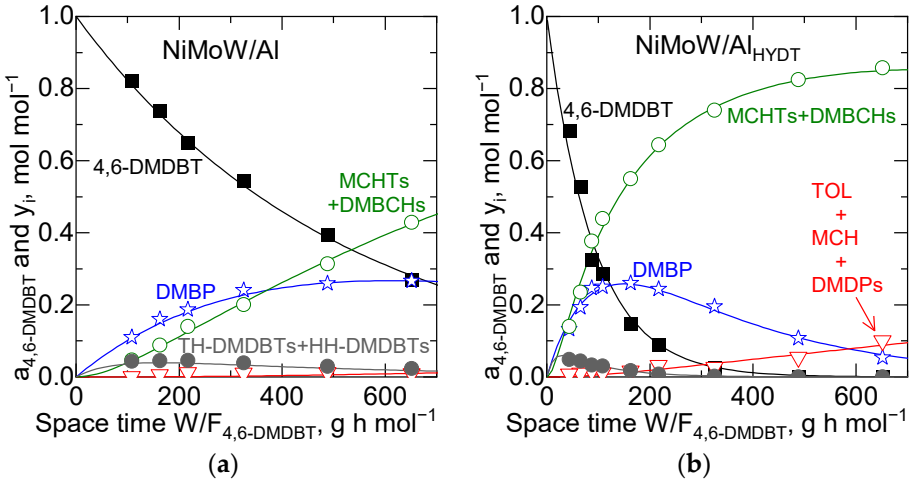

Figure 13. The simplified reaction product kinetic analysis (RPKA) of the 4,6-dimethyldibenzothiophene hydrodesulfurization at 360 °C and 5 MPa: (**a**) NiMoW/Al; (**b**) NiMoW/Al_{HYDT}. The solid lines were calculated by the system of Equation (3).

The direct desulfurization pathway of 4,6-DMDBT was given by the yield of dimethylbiphenyl (y_{DMBP}) and the rate constant k_{DDS} (Figure 13 and Table 4).

Table 4. The empirical pseudo-first-order rate constants of the 4,6-DMDBT hydrodesulfurization at 360 °C and 5 MPa according to the scheme in Figure 1 and system of Equation (3).

Catalyst	DDS and HYD Pathway of HDS Reaction				Cracking Reaction	
	k_{DDS}	k_{HYD1}	k_{HYD2}	k_{HYD3}	k_{CRA1}	k_{CRA2}
	mmol g^{-1} h^{-1}					
NiMoW/Al	1.19	0.75	13.98	1.34	0.01	0.06
NiMoW/Al_{HYDT}	4.92	6.14	73.41	3.47	0.16	0.17

The formation of hydrogenated intermediates tetrahydro- and hexahydro- dimethyldibenzothiophenes was described by k_{HYD1} and $y_{TH\text{-}DMBTs+HH\text{-}DMDBTs}$. The desulfurized products of this hydrogenation pathway were dimethylcyclohexyl-toluenes and dimethylbicyclohexyls ($y_{MCHTs+DMBCHs}$). They were preferentially formed by hydrodesulfurizing tetrahydro- and hexahydrodimethyldibenzo-thiophenes described by k_{HYD2}. Nevertheless, they were also partly formed by the hydrogenation of dimethylbiphenyl (k_{HYD3}). This less pronounced reaction is seen in RPKA over NiMoW/Al_{HYDT} at high space times in Figure 13b.

The least pronounced reaction on all catalysts was the cracking (CRA) of desulfurized C_{14} hydrocarbons to C_7 hydrocarbons described by k_{CRA1}, k_{CRA2} (Table 4), and $y_{TOL+MCH+DMCPs}$ (Figure 13). Yields of C_7 up to about 10% were only observed for the most active catalyst and the highest space–time in Figure 13b.

Figure 13 showed that the selectivity towards the reaction products at the same conversion of 4,6-DMDBT ($x_{4,6\text{-DMDBT}} = 1 - a_{4,6\text{-DMDBT}}$) was practically the same for all catalysts studied.

4. Discussion

The properties of tri-metallic catalysts in the hydrodesulfurization of organics can be significantly influenced by using a suitable support for the active components. As our study has shown, they depend very much on the support properties used. Mesoporous aluminas prepared by both the sol-gel method and its hydrothermal treatment differed not only in their physicochemical properties but also significantly affected the properties of the prepared tri-metallic catalysts.

Mesoporous alumina prepared by the sol-gel method using Al iso tri butoxide and hydrothermally treated (24 h at 150 °C) provided alumina characterized by a slightly lower surface area (217 m^2 g^{-1}) after calcination at 600 °C, smaller pore volume (0.47 cm^3 g^{-1}), and a somewhat smaller pore size (8.7 nm) than the conventional sol-gel alumina based on Al isopropoxide (without hydrothermal treatment) and calcined at 600 °C (surface area 232 m^2 g^{-1}, pore volume 0.52 cm^3 g^{-1} and pore size 9.0 nm). These differences in the porous structure of the two types of supports are not very large, but in other physical properties, the two types of alumina differed more significantly. In XRD measurements, hydrothermally treated alumina showed a significantly greater degree of crystallization than alumina that was only calcined. In the TEM images of the sol-gel alumina (Figure 4c,d), an organized mesoporous structure with completely regular pores was observed, while the hydrothermally treated sample had textural mesoporosity built up from small corrugated platelets, as previously observed in a sample prepared by a similar method by Lesaint et al. [15].

The properties of the calcined tri-metallics catalysts largely reflected the properties of the supports used. The porous structure of the catalysts was partially changed as a result of impregnation/calcination. In particular, the surface area of the catalysts, the volume, and the pore size were reduced, more so for the calcined sol-gel alumina than for the hydrothermally treated one due to the partial filling of the pores with active components.

No peaks of crystalline NiMo(W) oxides were observed on any of the XRD patterns, indicating they were amorphous on mesoporous alumina supports. The reduction peak of the Mo(W) species in the low-temperature region of the NiMoW/Al catalyst in Figure 5b had a low intensity. This indicates a low amount of easily reducible metal oxide species on the surface with weak interaction with the support. Thus, a poorer dispersion of the tri-metallic NiMoW components on the sol-gel alumina. XPS data of the calcined NiMoW/Al sample (Table 3) confirmed the lower amount of active metals on the surface for this sample. This agrees with the surface atomic concentrations found by XPS data (Table 3). However, the presence of W contributes to the appearance of broad reduction peaks at 545 and 615 °C in the catalysts, probably forming a mixed Mo-W oxide phase and thus facilitating the reduction of Mo species [23].

The XPS results of the sulfided NiMoW catalysts revealed that the degree of sulfidation and the number of active species are higher for the NiMoW/Al_{HYDT} catalyst than for the NiMoW/Al catalyst, which is consistent with the catalytic activity results.

The concordant trend in the TPR and XPS data (Figure 5b, Table 3) of the NiMoW/Al_{HYDT} catalyst shows better reducibility and a higher degree of sulfidation of Mo and W than that of the NiMoW/Al catalyst. After the catalytic tests, a slight decrease in the surface Ni/Al and Mo/Al ratios was observed for the NiMoW/Al catalyst, while these ratios remained unchanged for the NiMoW/Al_{HYDT} sample. This again points to a higher dispersion of the NiMoW phase on Al_{HYDT} γ-alumina.

From the experimental study, it is evident that sulfidation and catalytic reactions cause further textural and structural changes in the catalysts. Minor structural changes were found in the XRD patterns of NiMoW/Al_{HYDT} after the HDS reaction. The reflection of (002) at 14.4° was not observed in the used NiMoW/Al_{HYDT} catalyst. This result showed that the Mo(W)S_2 nanoparticles did not grow further along the c-axis under the reaction conditions in order to maintain the activity of the sample. Furthermore, the XPS data showed high atomic ratios of Mo/Al and W/Al in the sulfided and used NiMoW/Al_{HYDT} catalysts (Table 3) and high activity in the HDS of 4,6-DMDBT compared to NiMoW/Al. The high activity can be explained by the higher abundance of active Ni-Mo(W)-S_x species, the

optimal stacking degree, and the easier access of 4,6-DMDBT, a relatively bulky molecule, to the active centers in the large pores (7.5 nm) of the NiMoW/Al_{HYDT} catalyst. The size of the 4,6-DMDBT molecule (0.78 × 1.13 nm), a typical sulfur-containing intermediate, and the main HDS products were estimated from [29].

5. Conclusions

The preparation conditions of mesoporous alumina used as a support for tri-metallic NiMoW catalyst have a great influence on the metal-support interaction and catalytic activity. In this work, a novel highly active tri-metallic NiMoW/Al_{HYDT} HDS catalyst was prepared by impregnating NiMoW components on a hydrothermally synthesized mesoporous alumina support. The NiMoW/Al_{HYDT} catalyst was more efficient in HDS of 4,6-DMDBT than the NiMoW/Al catalyst prepared on alumina support obtained by the conventional sol-gel method. This is believed to be due to the combination of textural (pore size ~7.5 nm) and reducing properties, suitable metal-support interactions, and good dispersion of active nanocrystallites (slab length 2–4 nm) on alumina support prepared by hydrothermal method. The tri-metallic catalyst supported on conventional sol-gel alumina showed low conversion in both thiophene and 4,6-DMDBT hydrodesulfurization reactions due to the small pore size (~5 nm) and the strong interaction between the alumina surface and the active metals.

Author Contributions: Conceptualization, writing—original draft preparation, investigation, funding acquisition, R.P. and L.K.; TPR methodology, T.P.; XPS methodology, G.T.; XRD methodology, L.D.; HRTEM methodology, D.K.; writing, editing, supervision, K.J. All authors have read and agreed to the published version of the manuscript.

Funding: This research was funded by Scientific Cooperation Funds of Bulgarian and Czech Academies of Sciences Nos. IC-CZ/02/2023-2024 and BAS-23-01, respectively. Research equipment of Distributed Research Infrastructure INFRAMAT, part of the Bulgarian National Roadmap for Research Infrastructures, supported by the Bulgarian Ministry of Education and Science, was used in this investigation.

Data Availability Statement: The data will be made available on request.

Conflicts of Interest: The authors declare no conflict of interest.

References

1. Song, C. An overview of new approaches to deep desulfurization for ultra-clean gasoline, diesel fuel and jet fuel. *Catal. Today* **2003**, *86*, 211–263. [CrossRef]
2. Topsøe, H.; Clausen, B.S.; Massoth, F.E. *Hydrotreating Catalysts, Science and Technology*; Springer: Berlin/Heidelberg, Germany, 1996; pp. 22–24.
3. Yerga, R.M.N.; Pawelec, B.; Mota, N.; Huirache-Acuña, R. Hydrodesulfurization of Dibenzothiophene over Ni-Mo-W Sulfide Catalysts Supported on Sol-Gel Al_2O_3-CeO_2. *Materials* **2022**, *15*, 6780. [CrossRef] [PubMed]
4. Cervantes-Gaxiola, M.E.; Arroyo-Albiter, M.; Pérez-Larios, A.; Balbuena, P.B.; Espino-Valencia, J. Experimental and theoretical study of NiMoW, NiMo, and NiW sulfide catalysts supported on an Al-Ti-Mg mixed oxide during the hydrodesulfurization of dibenzothiophene. *Fuel* **2013**, *113*, 733–743. [CrossRef]
5. Shan, S.; Liu, H.; Yue, Y.; Shi, G.; Bao, F. Trimetallic WMoNi diesel ultra-deep hydrodesulfurization catalysts with enhanced synergism prepared from inorganic-organic hybrid nanocrystals. *J. Catal.* **2016**, *344*, 325–333. [CrossRef]
6. Castillo-Villalón, P.; Ramírez, J.J.; Cuevas, R.; Vázquez, P.; Castañeda, R. Influence of the support on the catalytic performance of Mo, CoMo, and NiMo catalysts supported on Al_2O_3 and TiO_2 during the HDS of thiophene, dibenzothiophene, or 4,6-dimethyldibenzothiophene. *Catal. Today* **2016**, *259*, 140–149. [CrossRef]
7. Garcia, E.D.; Chen, J.; Oliviero, E.; Oliviero, L.; Mauge, F. New insight into the support effect on HDS catalysts: Evidence for the role of Mo-support interaction on the MoS_2 slab morphology. *Appl. Catal. B* **2020**, *260*, 117975. [CrossRef]
8. Mendoza-Nieto, J.A.; de Oca, A.V.-M.; Calzada, L.A.; Klimova, T.E. Trimetallic NiMoW and CoMoW catalysts supported on SBA-15 modified with titania or zirconia for deep hydrodesulfurization. *Catal. Today* **2021**, *360*, 78–89. [CrossRef]
9. Alonso-Pérez, M.O.; Pawelec, B.; Zepeda, T.A.; Alonso-Nunez, G.; Nava, R.; Navarro, R.M.; Huirache-Acuña, R. Effect of the titanium incorporation method on the morphology and HDS activity of supported ternary Ni-Mo-W/SBA-16 catalysts. *Microporous Mesoporous Mater.* **2021**, *312*, 110779. [CrossRef]
10. Čejka, J. Organized mesoporous alumina: Synthesis, structure and potential in catalysis. *Appl. Catal. A* **2003**, *254*, 327–338. [CrossRef]

11. Kaluža, L.; Zdražil, M.; Žilková, N.; Čejka, J. High activity of highly loaded MoS_2 hydrodesulfurization catalysts supported on organised mesoporous alumina. *Catal. Commun.* **2002**, *3*, 151–157. [CrossRef]
12. Kaluža, L.; Gulková, D.; Šolcová, O.; Žilková, N.; Čejka, J. Hydrotreating catalysts supported on organized mesoporous alumina: Optimization of Mo deposition and promotional effects of Co and Ni. *Appl Catal. A* **2008**, *351*, 93–101. [CrossRef]
13. Bejenaru, N.; Lancelot, C.; Blanchard, P.; Lamonier, C.; Rouleau, L.; Payen, E.; Dumeignil, F.; Royer, S. Synthesis, Characterization, and Catalytic performances of novel CoMo hydrodesulfurization catalysts supported on mesoporous aluminas. *Chem. Mater.* **2009**, *21*, 522–533. [CrossRef]
14. Yuan, Q.; Yin, A.-X.; Sun, L.-D.; Zhang, Y.-W.; Duan, W.-T.; Liu, H.-C.; Yan, C.-H. Facile Synthesis for Ordered mesoporous γ-aluminas with high thermal stability. *J. Am. Chem. Soc.* **2008**, *130*, 3465–3472. [CrossRef] [PubMed]
15. Lesaint, C.; Glomm, W.R.; Borg, Ø.; Eri, S.; Rytter, E.; Øye, G. Synthesis and characterization of mesoporous alumina with large pore size and their performance in Fischer–Tropsch synthesis. *Appl. Catal. A* **2008**, *351*, 131–135. [CrossRef]
16. Thommes, M.; Kaneko, K.; Neimark, A.V.; Olivier, J.P.; Rodriguez-Reinoso, F.; Rouquerol, J.; Sing, K.S.W. IUPAC Technical Report. *Pure Appl. Chem.* **2015**, *87*, 1051–1069. [CrossRef]
17. Mendoza-Nieto, J.A.; Robles-Méndez, F.; Klimova, T.E. Support effect on the catalytic performance of tri-metallic NiMoW catalysts prepared with citric acid in HDS of dibenzothiophenes. *Catal. Today* **2015**, *250*, 47–59. [CrossRef]
18. Schoonheydt, R.A. Chemical Industries Series. In *Characterization of Heterogeneous Catalysts*; Delannay, F., Ed.; Marcel Dekker, Inc.: New York, NY, USA, 1984; Volume 15, pp. 125–185.
19. Zhang, Z.; Suo, J.; Zhang, X.; Li, S. Synthesis, characterization, and catalytic testing of W-MCM-41 mesoporous molecular sieves. *Appl. Catal. A* **1999**, *179*, 11–19. [CrossRef]
20. Huirache-Acuna, R.; Zepeda, T.A.; Vazquez, P.J.; Rivera-Munoz, E.M.; Maya-Yescas, R.; Pawelec, B.; Alonso-Nunez, G. The use of inorganic Al-HMS as a support for NiMoW sulfide HDS catalysts. *Inorg. Chim. Acta* **2021**, *524*, 120450. [CrossRef]
21. Ramírez, J.; Romualdo-Escobar, D.; Castillo-Villalón, P.; Gutiérrez-Alejandre, A. Improved NiMoSA catalysts: Analysis of EDTA post-treatment in the HDS of 4,6- DMDBT. *Catal. Today* **2020**, *349*, 168–177. [CrossRef]
22. Li, M.; Ihli, J.; Verheijen, M.A.; Holler, M.; Guizar-Sicairos, M.; Van Bokhoven, J.A.; Hensen, E.J.M.; Weber, T. Alumina-Supported NiMo Hydrotreating Catalysts Aspects of 3D Structure, Synthesis, and Activity. *J. Phys. Chem. C* **2022**, *126*, 18536–18549. [CrossRef]
23. Mendoza-Nieto, J.A.; Vera-Vallejo, O.; Escobar-Alarcon, L.; Solis-Casados, D.A.; Klimova, T. Development of new trimetallic NiMoW catalysts supported on SBA-15 for deep hydrodesulfurization. *Fuel* **2013**, *110*, 268–277. [CrossRef]
24. Zuo, D.; Li, D.; Nie, H.; Shi, Y.; Lacroix, M.; Vrinat, M. Acid–base properties of NiW/Al_2O_3 sulfided catalysts: Relationship with hydrogenation, isomerization and hydrodesulfurization reactions. *J. Mol. Catal. A Chem.* **2004**, *211*, 179–189. [CrossRef]
25. Yin, C.; Wang, Y.; Xue, S.; Liu, H.; Li, H.; Liu, C. Influence of sulfidation conditions on morphology and hydrotreating performance of unsupported Ni–Mo–W catalysts. *Fuel* **2016**, *175*, 13–19. [CrossRef]
26. Amaya, S.L.; Alonso-Núñez, G.; Cruz-Reyes, J.; Fuentes, S.; Echavarría, A. In-fluence of the sulfidation temperature in a NiMoW catalyst derived from layered structure $(NH_4)Ni_2OH(H_2O)(MoO_4)_2$. *Fuel* **2015**, *139*, 575–583. [CrossRef]
27. Hensen, E.J.M.; Van der Meer, Y.; Van Veen, J.A.R.; Niemantsverdriet, J.W. Insight into the formation of the active phases in supported NiW hydrotreating catalysts. *Appl. Catal. A* **2007**, *322*, 16–32. [CrossRef]
28. Lizama, L.; Klimova, T. Highly active deep HDS catalysts prepared using Mo and W heteropolyacids supported on SBA-15. *Appl. Catal. B* **2008**, *82*, 139–150. [CrossRef]
29. Fu, W.; Zhang, L.; Tang, T.; Ke, Q.; Wang, S.; Hu, J.; Fang, G.; Li, J.; Xiao, F.-S. Extraordinarily High Activity in the Hydrodesulfurization of 4,6-Dimethyldibenzothiophene over Pd Supported on Mesoporous Zeolite Y. *J. Am. Chem. Soc.* **2011**, *133*, 15346–15349. [CrossRef]